



## Direct Imaging of Electron States in Open Quantum Dots

N. Aoki,<sup>1</sup> R. Brunner,<sup>2</sup> A. M. Burke,<sup>3,4</sup> R. Akis,<sup>3</sup> R. Meisels,<sup>2</sup> D. K. Ferry,<sup>3</sup> and Y. Ochiai<sup>1</sup>

<sup>1</sup>*Graduate School of Advanced Integration Science, Chiba University, 1-33 Yayoi-cho, Inage-ku, Chiba 263-8522, Japan*

<sup>2</sup>*Department of Physics, Montanuniversitaet Leoben, Franz Josef Str.18, Leoben A-8700, Austria*

<sup>3</sup>*Department of Electrical Engineering and Center for Solid State Electronics Research, Arizona State University, Tempe, Arizona 85287-5706, USA*

<sup>4</sup>*School of Physics, The University of New South Wales, Sydney 2052, Australia*

(Received 8 September 2011; published 30 March 2012)

We use scanning gate microscopy to probe the ballistic motion of electrons within an open GaAs/AlGaAs quantum dot. Conductance maps are recorded by scanning a biased tip over the open quantum dot while a magnetic field is applied. We show that, for specific magnetic fields, the measured conductance images resemble the classical transmitted and backscattered trajectories and their quantum mechanical analogue. In addition, we prove experimentally, with this direct measurement technique, the existence of pointer states. The demonstrated direct imaging technique is essential for the fundamental understanding of wave function scarring and quantum decoherence theory.

DOI: 10.1103/PhysRevLett.108.136804

PACS numbers: 73.21.La, 68.37.Ps, 73.23.Ad, 73.63.-b

The concept of measurement plays a crucial role in quantum mechanics. It proved to be a great source of difficulty, as has been found in the Einstein-Podolsky-Rosen paradox [1] or the Schrödinger's cat paradox [2]. The readout of information from a quantum mechanical system with a classical apparatus presumes the knowledge of the transition between the classical and quantum mechanical world [3]. Open quantum dots (QD), exhibit interesting laboratories in which to study this transition [4–7]. Open QDs, in contrast to closed quantum dots, for example, [8] are strongly coupled to the nearby electron reservoirs or environment. The coupling to the environment causing perturbation is mediated by a pair of constrictions without forming tunnel barriers. From the classical point of view, the dynamics of such open QD is mixed [9]. The chaotic trajectories within the mixed phase space correspond to the current carrying quantum states heavily damped by the coupling to the environment, whereas the regular trajectories correspond to states robust against the environmental coupling. In general, the coupling induced selection leads to a preferred set of states known as pointer states. Pointer states eventually correspond to classical states that are persistent to environmental monitoring during the measurement process [3]. They have been investigated in nanostructures so far by direct transport measurements [4–7] and indirect imaging by using the Fourier transformed scanning probe technique [10]. In the latter, additional environmental perturbation is induced to the open quantum dot by scanning a biased atomic force microscope (AFM) tip over the area of interest.

Scanning gate microscopy (SGM), in combination with transport measurements, can provide an interesting tool to image the motion of electrons in quantum systems [11–14]. However, the direct imaging of specific features from single scarred wave functions in open QDs is difficult

[14] and has not been demonstrated so far. It has been theoretically argued for an open QD, however using a hard-wall potential, that by introducing a tip the resulting shift of conductance resonances make a detection of the unperturbed probability density challenging [15]. Nevertheless, the direct imaging of single wave functions, including their classical analogue, and the experimental investigation of pointer states in open quantum dots is important since it may lead to gaining novel information about wave function scarring [16], the quantum to classical transition, and dissipation in quantum systems [3,17].

Here, we use a cryogenic SGM to probe the ballistic motion of electrons within an open GaAs/AlGaAs QD. Conductance maps are recorded using a biased, swept tip in a magnetic field. We show for specific values of the magnetic field, conductance images that resemble classical transmitted and backscattered trajectories as well as their quantum mechanical analog. In addition, we bring further experimental evidence that pointer states exist in open quantum dots by directly visualizing the robustness of the states in the conductance maps.

We expect the effective size of the open QD to be  $1.0 \mu\text{m} \times 1.0 \mu\text{m}$  although its lithographic design is  $1.5 \mu\text{m} \times 1.5 \mu\text{m}$  as shown by the AFM image of Fig. 1(a) [18]. The carrier concentration and mobility are  $4.8 \times 10^{11}/\text{cm}^2$  and  $4.2 \times 10^5 \text{ cm}^2/\text{V s}$ , respectively, and the corresponding mean free path ( $l_0$ ) is  $4.5 \mu\text{m}$  at 4.2 K. Since the dot size is much smaller than  $l_0$ , the transport in the open QD can be considered as ballistic.

During the SGM measurement, the tip is mainly biased with  $-6 \text{ V}$  in dc and scanned in the  $x$ - $y$  plane 50 nm above the surface of the wafer, without feedback loop, with slope correction (the  $z$  is constant from the surface plane of the sample but not following the topographic structure). The resistance across the open QD is measured in a 4-terminal

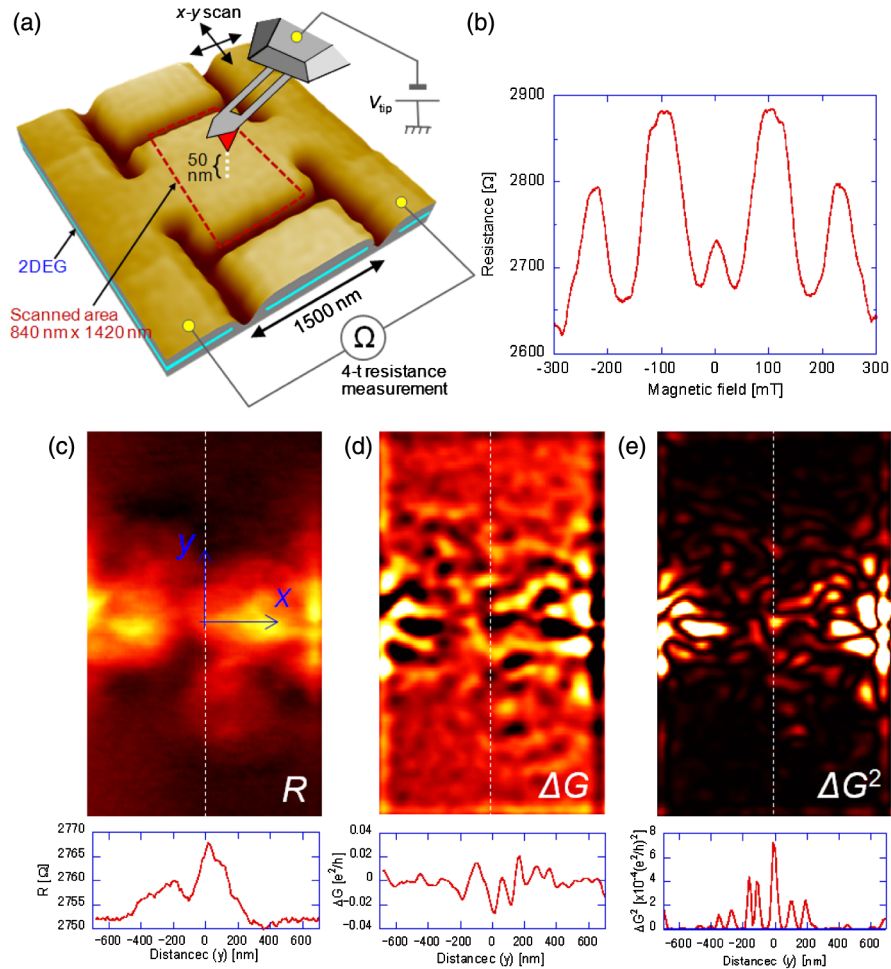


FIG. 1 (color online). (a) AFM image of the open QD sample fabricated by electron beam lithography and wet etching. The dotted rectangular ( $860 \text{ nm} \times 1420 \text{ nm}$ ) region highlights the scanning area in the SGM observations. On top of the QD, a tip is applied in lift mode with a certain distance ( $50 \text{ nm}$ ) with respect to the wafer surface. The tip is biased typically with  $-6 \text{ V}$  in dc and causes depletion in the two-dimensional electron gas plane. Note that both perpendicular sides of the dot can be used as side gates. (b) Magneto resistance of the open QD measured without a biased tip. At certain magnetic field values, maxima (at  $B = 100 \text{ mT}$ ,  $B = 240 \text{ mT}$ ) and minima ( $B = 180 \text{ mT}$ ) arise. SGM image shows (c) the change of the resistance  $R$  across the open QD (bright: high  $R$ ), (d) the variation of the conductance  $\Delta G$  (bright: positive  $\Delta G$ , dark: negative  $\Delta G$ ), and (e)  $\Delta G^2$  corresponding to the square of the conductance variation  $\Delta G$  (bright: high  $\Delta G^2$ ). Below: The corresponding line profiles for  $R$ ,  $\Delta G$ , and  $\Delta G^2$  are shown for clarity.

( $4$ - $t$ ) configuration using lock-in amplifiers. The data including the information of the tip position are stored in a computer at the same time. The magnetic field ( $B$ ) is applied perpendicular to the sample surface. Further details of the experimental procedure are given in Ref. [19]. At first, we measure the magneto resistance across the open QD at  $0.3 \text{ K}$  in the direct transport measurement mode [Fig. 1(b)]. We obtain maxima and minima in the magneto resistance at certain magnetic fields. Small conductance oscillations are superimposed on the trace, as discussed later. Such transport characteristics in the magneto resistance have also been reported and explained in ballistic open QD arrays [6,20].

In Figs. 1(c)–1(e), typical SGM images observed in the open QD are shown with different image display possibilities, e.g., to show the change of the resistance  $R$  [Fig. 1(c)], the conductance fluctuations components  $\Delta G$

[Fig. 1(d)], and the absolute value of the variation of conductance fluctuation  $\Delta G^2$  [Fig. 1(e)]. The conductance fluctuation components  $\Delta G$  are obtained by subtracting the smoothed background (same effect as a low-pass filtered image) from an inverse ( $1/R$ ) of the original SGM image ( $R$ ). This process is equivalent to applying a high-pass filter to the  $1/R$  image. By taking the square of the  $\Delta G$  value, we are able to resolve the absolute value  $\Delta G^2$ . Below the images, the line profiles for each display possibility are shown.

In Fig. 2, we present the  $\Delta G^2$  images obtained at  $B = 0$ ,  $100$ ,  $180$ , and  $240 \text{ mT}$  [21]. The values correspond to the minima and maxima of the magneto-resistance trace shown in Fig. 1(b). Model calculations are performed using a soft-wall as opposed to a hard-wall potential. Note, that this potential gives the closest fit to the magneto-resistance

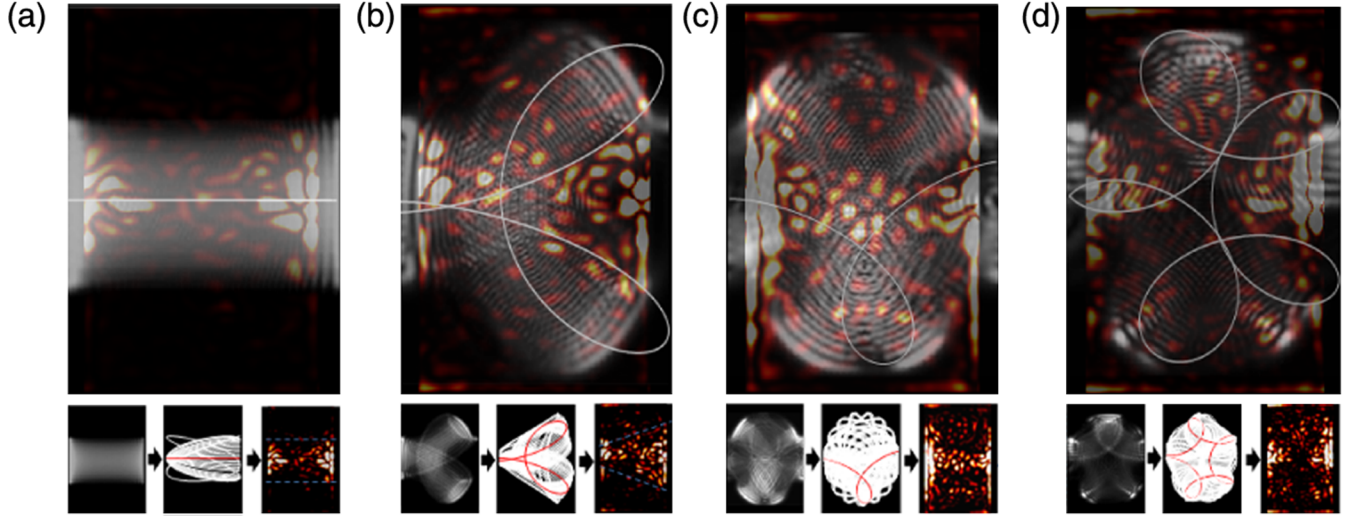


FIG. 2 (color online). Comparison of classical trajectories, scarred wave function, and  $\Delta G^2$  images at different magnetic field values. Above: A single featured trajectory and probability density superimposed on the  $\Delta G^2$  image. Below: Trajectory calculated for various entrance angles (about  $-90^\circ$  to  $+90^\circ$ ) including the featured trajectory (in red), probability density, and  $\Delta G^2$  image, all shown as separated figures. Dashed lines in the image are used as a guide for the eye. (a)  $B = 0$  mT, featured single trajectory with an entrance angle of  $0^\circ$ . (b)  $B = 100$  mT, featured single trajectory with an entrance angle of  $0^\circ$ . (c)  $B = 180$  mT, featured single trajectory with an entrance angle of  $-5.7^\circ$ . (d)  $B = 240$  mT, featured single trajectory with an entrance angle of  $17.2^\circ$ . Color code: High and low probability density correspond to grey and black, respectively. High and low  $\Delta G^2$  corresponds to bright and dark, respectively. The size of each panel is  $1000 \text{ nm} \times 1500 \text{ nm}$ .

trace in Fig. 1(b). The classical trajectories are obtained by solving the classical equation of motion in the open QD assuming ballistic transport. We adjust the size of the dot in the simulation to the approximated dimensions shown in Fig. 1(a). From the electron concentration, we evaluate the Fermi energy  $E_F = 17.2 \text{ meV}$  and  $\omega_0 = 6.0 \times 10^{11} \text{ s}^{-1}$  for an extension of the dot in  $x$  of  $0.5 \mu\text{m}$ . In addition, we use a small anisotropy ( $\omega_{0x}/\omega_{0y} = 0.7$ ). The anisotropy is used to adjust exactly the magnetic field values from the maxima and minima in the calculations to the experimentally obtained result [Fig. 1(c)] and to meet the condition one obtains from fully self-consistent calculations [22]. In addition, we calculate for the presented open QD the quantum mechanical probability density. It is obtained using an iterative solution to the Lippmann-Schwinger equation [23]. Figure 3 shows for the different magnetic field values, the probability density, the calculated classical trajectories for various entrance angles, and the  $\Delta G^2$  images. The calculated results resemble trajectories and wave functions which emerge from hybridization between dot and environment states. At  $B = 0$  and  $180 \text{ mT}$  the trajectories show mainly transmitted properties, and at  $100$  and  $240 \text{ mT}$  they show backscattered properties. The trajectories at  $B = 0$  and  $100 \text{ mT}$  show strong insensitivity to their starting conditions over the whole angle spectrum. Here, clearly, quantum to classical correspondence is achieved. However, the situation changes by increasing the magnetic field. At  $180 \text{ mT}$  and  $240 \text{ mT}$ , the trajectories are more sensitive to the entrance angle and resemble less the pure transmitted and backscattering condition, respectively,

[18] for different entrance angles. Now, we directly compare the results from the calculation with the evaluated images. Like the calculated wave functions and trajectories, the corresponding  $\Delta G^2$  images presented in Figs. 2(a)–2(d) also demonstrate sensitivity on the magnetic field. In addition, the  $\Delta G^2$  images for the different magnetic field values resemble quite well the calculated single trajectories and wave functions, especially for the lower magnetic field values at  $B = 0$  and  $100 \text{ mT}$ . The measured  $\Delta G^2$  intensity is strongly increased at certain regions within the scan area. In our observation, tip induced resonances in  $\Delta G^2$  appear keenly where the tip unperturbed quantum mechanical density probability is maximal. Small or even no conductance resonances appear where the probability density is low. At higher magnetic fields the quality of the measured images degrades. Usually, one would consider that the scanning AFM tip would completely destroy the original trajectory or single scarred wave function due to the induced coupling to the current carrying states [15]. However, the grade of how much a trajectory is perturbed will depend on its stability within the phase space. The used soft-wall potential results in a high stability of the commensurate trajectories in phase space, especially for the lower magnetic field [Figs. 2(a) and 2(b)] [7,18]. Therefore, we are able to image rather specific features of the single scarred wave function and trajectories for different magnetic field values than just general features as demonstrated previously [14]. At higher magnetic fields the stability of the commensurate trajectories decreases

and coupling to current carrying states, due to perturbation, becomes more likely. Here, as shown in Figs. 2(c) and 2(d), the correspondence between image and calculation becomes less evident.

Now, we provide evidence for the existence of pointer states. Therefore, we investigate the perturbation in the QD induced by the coupling of the dot to the electron reservoirs via the constrictions as well as by the tip. In addition to the measured maxima and minima [Fig. 1(c)], we also observe magneto-conductance oscillations [Fig. 3] superimposed on the magneto-resistance traces. The oscillation components are obtained by subtracting the smoothed background from the magneto-conductance curve. The oscillations are quasiperiodic in magnetic field, well reproduced for different sweep directions of the magnetic field and exhibit a Fano line shape. The Fano line shape of the resonances can be explained by phase space tunneling between regions in the classical phase space corresponding to regular and chaotic trajectories [4,6,7]. In Fig. 3, we compare the conductance oscillations with and without tip

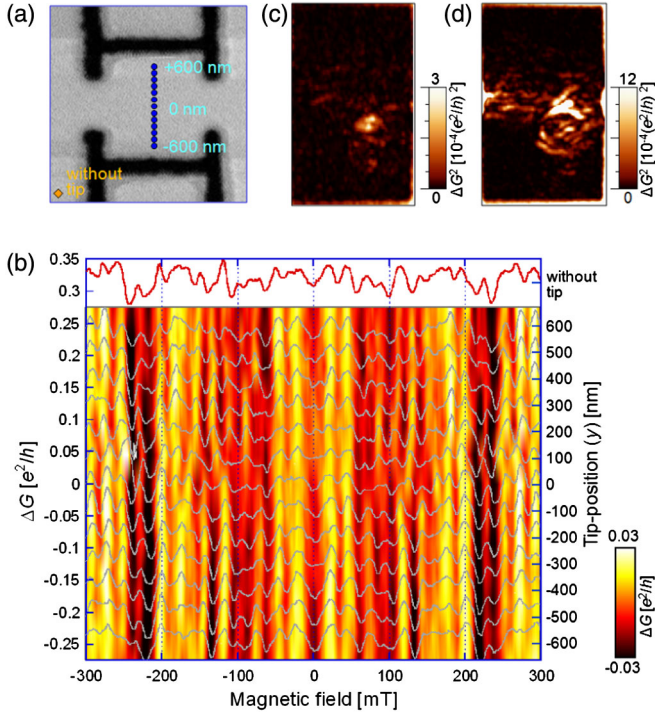


FIG. 3 (color online). (a) Topographic image from the open QD. Circles show schematically the various measurement positions in  $y$  between  $-600$  and  $+600$  nm at  $x = 0$  nm. (b) Magneto-conductance oscillations and the contour plot measured at the different tip positions shown in (a). Each curve is plotted with certain offsets. High and low conductance corresponds to bright and dark, respectively, as shown in a color-scale bar. The amplitude of the conductance oscillations curve is within  $\pm 0.02e^2/h$  which is the same order of conductance oscillations without the tip shown at the top. (c) and (d) are  $\Delta G^2$  images obtained with  $V_{tip} = -3$  V and  $-6$  V, respectively, at  $B = 0$  T and  $V_s = 0$  V.

induced potential (above) for the same magnetic field region. This will give us a measure of the stability of the regular trajectories in the sea of chaos while a tip is introduced. Figure 3(a) shows the varying positions of the tip in the open QD. We positioned the tip at the dot center (taken to correspond to  $x = 0$  nm) within the open QD, moved it in increments of  $y$  of 100 nm between  $+600$  to  $-600$  nm, and measured the magneto-conductance oscillations from  $-300$  to  $+300$  mT [Fig. 3(b)]. In Fig. 3(b), the magnetic field positions of the conductance resonances for the different tip positions and in direct comparison to the measurement without the tip are mainly preserved, indicating a high stability of the states connected to the conductance resonances.

Further, we investigate in Figs. 3(c) and 3(d) the effect of the tip voltage on the conductance resonance, while the coupling to the electron reservoirs is set constant. Both figures show a high response in the  $\Delta G^2$  image within a certain area. The distribution of the conductance resonance for  $-3$  V and  $-6$  V in Figs. 3(c) and 3(d), respectively, remains. This again indicates that certain states remain robust in the open QD although a tip is present.

Next, we change the coupling strength of the open QD to the electron reservoirs [Fig. 4]. Therefore, we measure directly  $\Delta G^2$  images [Figs. 4(a)–4(d)] for different side

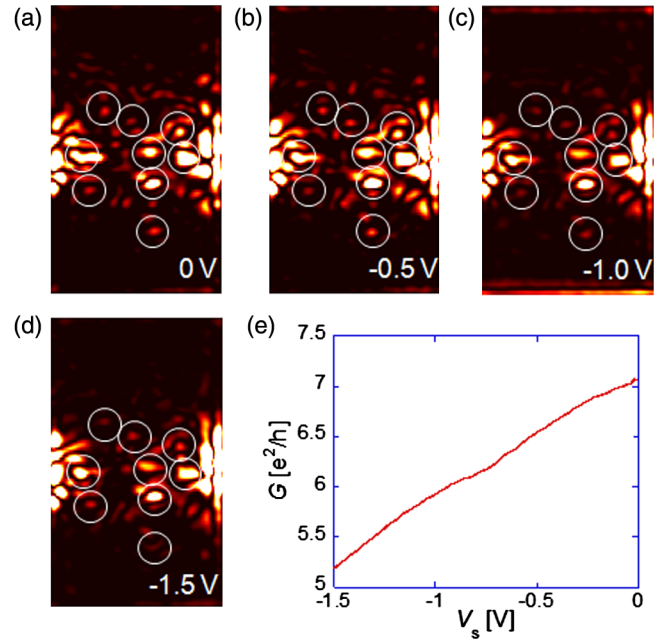


FIG. 4 (color online).  $\Delta G^2$  images obtained at zero magnetic field for different side gate voltages of  $V_s =$  (a) 0 V, (b)  $-0.5$  V, (c)  $-1.0$  V, and (d)  $-1.5$  V, respectively. These figures are plot in the same color scale. White circles show robust spots up to  $-1.5$  V. (e) Conductance  $G$  across the open QD as a function of the side gate voltage  $V_s$ . By increasing the negative voltage on the side gate, the conductance decrease due to depletion at the constriction regions. An indication that a less negative  $V_s$  is related to a stronger coupling to the environment.

gate voltage ( $V_s$ ) but constant tip potential of  $-6$  V at  $B = 0$  mT. As we change  $V_s$ , the conductance through the dot decreases as shown in Fig. 4(e) due to the depletion at the two constriction regions. The bright spots in the  $\Delta G^2$  images [Figs. 4(a)–4(d)] which indicate a high  $\Delta G^2$  response, are preserved for different  $V_s$ .

The observed robustness of the conductance resonances in Figs. 3 and 4 implies that the corresponding states must be orthogonal to the plurality of states in the system. Indeed, this is in correspondence with what has been shown previously for the wave functions corresponding to the Fano resonances in open quantum dots [4]. This orthogonality between the robust states and other states is presumed to result from einselection [3]. The environment induces superselection rules; thus, pointer states emerge [3]. Therefore, it consequently seems that pointer states in the investigated open quantum dot are detected by our approach.

In conclusion, we demonstrate a new approach to probe the carrier dynamics in an open QD by using SGM technique. We show the possibility to record conductance maps in an open QD while a magnetic field is applied. The demonstrated technique is sensitive to probe the characteristic of single wave functions and trajectories in the magnetic field. Because of the softness of the potential certain trajectories show a high stability in the phase space for certain magnetic fields. Therefore, the obtained  $\Delta G^2$  images reveal not only general features of closed-looped orbits or states but rather specific features of single scarred wave functions and trajectories which arise from the hybridization between dot and environment states. The study of the coupling from the QD to the environment gave further evidence that pointer states can be experimentally detected within open QDs. Finally, we propose that our direct imaging technique will be highly valuable for the deeper understanding of quantum decoherence theory [13] and wave function scarring [12].

We would like to thank F. Kuchar and J. Oswald for fruitful discussions. This work is supported in part by Grants-in-Aid for Scientific Research from JSPS

(19054016, 19204030, and 16656007), Core-to-Core program, and Chiba University Global COE Program (G-03).

- 
- [1] A. Einstein, B. Podolsky, and N. Rosen, *Phys. Rev.* **47**, 777 (1935).
  - [2] E. Schrödinger, *Naturwissenschaften* **23**, 807 (1935); **23**, 823 (1935); **23**, 844 (1935).
  - [3] W.H. Zurek, *Rev. Mod. Phys.* **75**, 715 (2003).
  - [4] D.K. Ferry, R. Akis, and J.P. Bird, *Phys. Rev. Lett.* **93**, 026803 (2004).
  - [5] D.K. Ferry *et al.*, *Semicond. Sci. Technol.* **26**, 043001 (2011).
  - [6] R. Brunner *et al.*, *Phys. Rev. Lett.* **101**, 024102 (2008).
  - [7] R. Brunner *et al.*, *Phys. Rev. Lett.* **98**, 204101 (2007).
  - [8] R. Brunner *et al.*, *Phys. Rev. Lett.* **107**, 146801 (2011).
  - [9] R. Ketzmerick, *Phys. Rev. B* **54**, 10841 (1996); A. Burke *et al.*, *J. Phys. Condens. Matter* **21**, 212201 (2009).
  - [10] A. Burke *et al.*, *Phys. Rev. Lett.* **104**, 176801 (2010).
  - [11] M. A. Topinka *et al.*, *Science* **289**, 2323 (2000).
  - [12] F. Martins *et al.*, *Phys. Rev. Lett.* **99**, 136807 (2007).
  - [13] A. Pioda *et al.*, *Phys. Rev. Lett.* **93**, 216801 (2004).
  - [14] R. Crook *et al.*, *Phys. Rev. Lett.* **91**, 246803 (2003).
  - [15] M. Mendoza and P.A. Schulz, *Phys. Rev. B* **71**, 245303 (2005).
  - [16] R. Akis, D.K. Ferry, and J.P. Bird, *Phys. Rev. Lett.* **79**, 123 (1997).
  - [17] J.A. Wheeler and W.H. Zurek, *Quantum Theory and Measurement*, edited by J.A. Wheeler and W.H. Zurek (Princeton University Press, Princeton, 1983).
  - [18] See Fig. 1S in Supplemental Material at <http://link.aps.org/supplemental/10.1103/PhysRevLett.108.136804>.
  - [19] N. Aoki *et al.*, *Phys. Rev. B* **72**, 155327 (2005); *Appl. Phys. Lett.* **87**, 223501 (2005).
  - [20] R. Akis *et al.*, *Phys. Rev. B* **60**, 2680 (1999).
  - [21] We confirmed that the fluctuations observed in the SGM image are completely reproducible and appear also by inverting the magnetic field.
  - [22] R. Akis *et al.*, in *Electron Transport in Quantum Dots*, edited by J.P. Bird (Kluwer, Dordrecht, 2003).
  - [23] R. Akis, D. K. Ferry, and J. P. Bird, *Phys. Rev. B* **54**, 17705 (1996).